Engineering Iron-Nickel Nanoparticles for Magnetically-Induced CO2 Methanation in Continuous Flow

Déborah de Masi, Juan Manuel Asensio, Pier-Francesco Fazzini, Lise-Marie Lacroix, Bruno Chaudret

Engineering Iron-Nickel Nanoparticles for Magnetically-Induced CO_2 Methanation in Continuous Flow

Déborah De Masi, Juan M. Asensio, Pier-Francesco Fazzini, Lise-Marie Lacroix, Bruno Chaudret**

LPCNO, Université de Toulouse, CNRS, INSA, UPS, 135 avenue de Rangueil, 31077 Toulouse, France.

*Dr Juan M. Asensio: asensior@ insa-toulouse.fr

*Dr. Bruno Chaudret: chaudret@insa-toulouse.fr

ABSTRACT. Induction heating of magnetic nanoparticles (NPs) has been recently explored as a new methodology to activate heterogeneous catalytic reactions. This approach requires the design and the synthesis of nano-objects displaying both a high heating power and an excellent catalytic activity. Here, using a surface engineering approach, we report for the first time the use of bimetallic NPs for magnetically-induced CO_2 methanation which acts both as heating agent and as catalyst. Thus, we describe the organometallic synthesis of $Fe_{30}Ni_{70}$ NPs, displaying high heating powers at low magnetic field amplitudes. These NPs are active but only slightly selective for CH4 after deposition on SirAlOx due to the presence of an iron rich shell (25 mL·min^{-1}, 25 mT, 300 kHz, conversion 71%, methane selectivity 65%). Remarkably, a proper surface engineering consisting in depositing a thin Ni layer leads to $Fe_{30}Ni_{70}$@Ni NPs displaying a very high activity for CO_2 hydrogenation and a full selectivity. For the first time, a quantitative yield in methane is obtained at low magnetic field and mild conditions (25 mL·min^{-1}, 19 mT, 300 kHz, conversion 100%, methane selectivity 100%).

INTRODUCTION

Magnetic induction has recently appeared as an alternative heating source for heterogeneous catalytic reactions [1–9]. It consists in applying high frequency alternating magnetic field to ferromagnetic materials to release heat through hysteresis losses. The target temperature is reached within few seconds and the energy is directly transferred inside the material without the need for heating the whole reactor system. This technology appeared first as an engineer solution for fast heating catalytic reactors, making use either of the walls of the reactor [10–12] or from heating elements embedded inside such as iron balls or ferrite micro-particles.[1,13,14] In our group, we have demonstrated the possibility to magnetically induce CO_2 methanation in a continuous-flow reactor using core-shell NPs consisting of Ni or Ru coated iron-carbide cores displaying high heating properties.[2,4] However, a modest CO_2 conversion (50%) was achieved with a CH_4 yield of 15%. The spatial separation of the heating agent and the catalyst, by depositing $Fe_{2.2}C$ NPs on an inorganic support previously impregnated Ru or Ni NPs, led to CH4 yields higher than 90% at low magnetic field (ca; 20 mT).[4,5] Almost simultaneously, Mortensen *et al.*[15,16] and Varsano *et al.*[17] demonstrated that NiCo NPs could be used as both an heating agent and a catalyst for steam methane reforming under magnetic field, leading to excellent catalytic results (95% of H2 yield). In parallel, induction heating of ferromagnetic iron oxide-based NPs has been used to heat reactions in solution.[18–21] In this case, NPs could be only used as heating agents or as catalysts. In our group, we reported that a close contact between an heating agent and a catalyst (FeC@Ru NPs) allowed for the first time to perform high-temperature catalysis such as hydrodeoxygenation of biomass platform molecules in solution.[22]

The quasi instantaneous nature of magnetic heating seems well-adapted to the storage of intermittent energy, a promising solution being CO_2 methanation.[23–25] A large variety of catalysts has been investigated (Ni, Ru, Fe, Rh),[12,13] but Ni based catalysts are the most largely employed because of their high performance and low cost.[23] It has however

previously been proposed through DFT calculations that Fe-Ni catalysts are more active than monometallic catalysts for CO_2 methanation since they combine good CO adsorption and CO dissociation.[26–28] Accordingly, Tian *et al.*[29] reported that a Ni–Fe/γ-Al_2O_3 catalyst led to a CO_2 conversion near 100% under moderate pressure (3.0 MPa) with a CH_4 selectivity of 99%. Moreover, FeNi alloys display a low anisotropy and a sufficient saturation magnetization, making this material a good candidate to reach high temperatures under magnetic excitation at low field amplitude. FeNi NPs are usually synthesized by hydrothermal reduction but suffer from a lack of size and shape control.[30,31] An organometallic approach has been explored in our group but led to particles of small size.[32] We therefore turned to a methodology displaying similarities with the one recently reported for Fe-Co NPs.[33] In this study, we describe the synthesis of $FeNi_3$ NPs displaying both a high heating capacity and a remarkable catalytic activity leading to a fully selective conversion of CO_2 into methane at low magnetic field.

Bimetallic $Fe_{30}Ni_{70}$ NPs were synthesized by co-decomposition of $\{Fe[N(SiMe_3)_2]_2\}_2$ and $Ni[^iPrNC(CH_3)N^iPr]_2$ under 3 bars H_2 using palmitic acid (1.8 eq. per Fe complex) as stabilizer. First, a scope of the synthetic conditions was performed, varying the Ni:Fe ratio, reaction temperature and time. Transmission Electron Microscopy (TEM) images, chemical composition and Specific Absorption Rate (SAR) of the resulting different NPs are shown in Table S1 and Fig S1 in the Supporting Information. NPs ranging from 14.4 nm to 22.3 nm were obtained with Specific Absorption Rate (SAR) values ranging with the NP size from 200 $W \cdot g^{-1}$ to 820 $W \cdot g^{-1}$ at 47 mT and 93 kHz. Such a size dependence on the heating capability has been previously reported on other materials.[34] By reacting a 5:1 Ni:Fe ratio at 150°C during 24 h, FeNi NPs with a mean size of 17.3 ± 2.2 nm (Fig S1-d). were obtained. High-Resolution TEM (HR-TEM) analyses reveal that the NPs are polycrystalline and adopt the expected fcc structure (Figure S2), as further confirmed by powder X-Ray Diffraction (XRD, see Fig 1a). Chemical

analyses using Inductively Coupled Plasma-Mass Spectrometry (ICP-MS) and Scanning Electron Microscopy (SEM) coupled to Energy Dispersive X-ray Spectroscopy (EDX) (Figure S3) evidenced a global composition of 28 ± 1 Fe wt% and 72 ± 1 Ni wt%. We will therefore refer to the NPs from now on as $Fe_{30}Ni_{70}$ NPs. Local distribution of Fe and Ni was investigated by Scanning TEM coupled to EDX, revealing a Fe-rich surface in most of the NPs (Figure S4). Such chemical inhomogeneity was confirmed by Electron Energy Loss Spectroscopy (EELS) (Figure S5). Indeed, further analysis of individual NPs showed a chemical composition profile which fits with a $FeNi_3$@Fe_3Ni structure (Figure S6). The chemical distribution within NPs **1** was further studied by Mössbauer spectroscopy (Figure S8). The spectrum recorded at 77 K displays a broad sextet which can be attributed to several chemical environments of the Fe atoms. The major contributions were found for hyperfine fields between 28 and 32 T corresponding to FeNix structures.[35] The hyperfine field at 28 T can be attributed to FeNi3 alloy and corresponds to ca. 30% of the sample. Additionally, some hyperfine field contributions characteristic of Fe(0) could be observed at 34 T, likely due to the Fe shell at the surface of the NPs. The absence of hyperfine fields at 42-44 T, characteristic of FeOx environment revealed the metallic character of the NPs and the absence of any oxide shell.

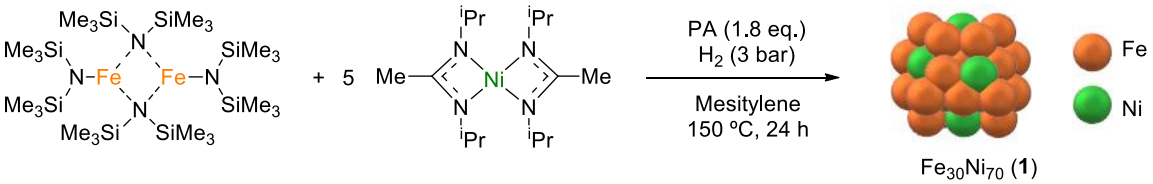

Scheme 1. Synthesis of $Fe_{30}Ni_{70}$ NPs **1** by co-decomposition of $\{Fe[N(SiMe_3)_2]_2\}_2$ and $Ni[^iPrNC(CH_3)N^iPr]_2$ under a H_2 atmosphere.

The magnetic properties of **1** were determined by Vibrating Sample Magnetometer, (VSM, see Fig 1b). At 300 K, the NPs are superparamagnetic; and they display a saturation magnetization value of 80 $A \cdot m^2 \cdot kg^{-1}$ in good agreement with the bulk value reported for this composition.[36]

After cooling down to 5 K under an applied field of 3T, NPs **1** display a low coercive field (μ0Hc = 3.4 mT) without any sign of *exchange bias*, thus confirming the absence of oxidation (Fig S7).[37] The SAR of the NPs measured at 47 mT and 93 kHz was 600 $W \cdot g^{-1}$ (Fig 1c).

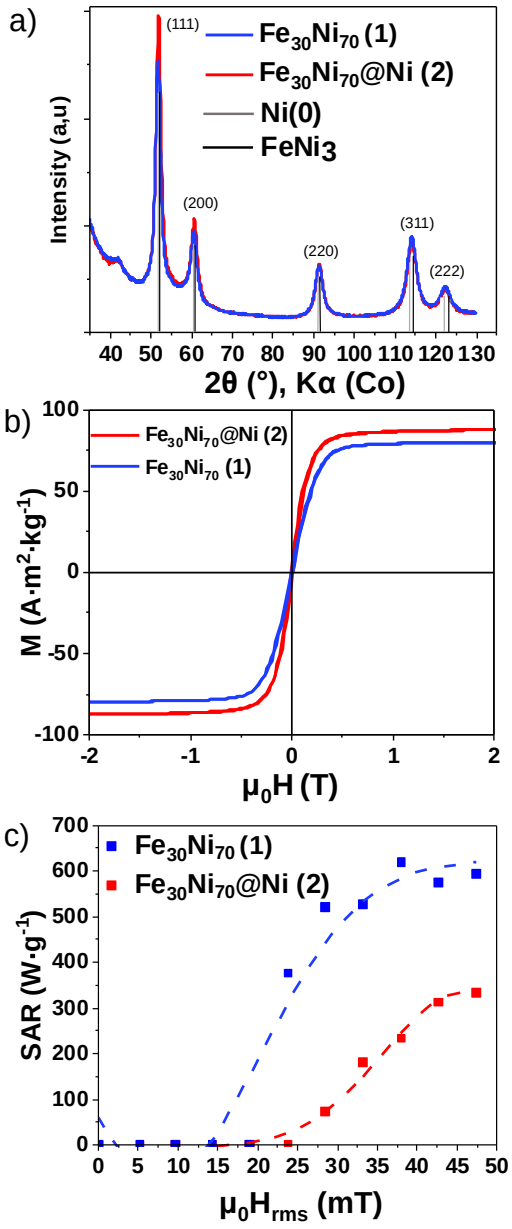

Figure 1. a) X-ray diffraction, b) magnetic hysteresis loop at 300 K and c) heating power measurements at 93 kHz and μ_0Hrms = 0-57 mT for $Fe_{30}Ni_{70}$ NPs **1** and $Fe_{30}Ni_{70}$@Ni NPs **2**.

NPs **1** were immobilized on SiRAlOx (see Fig S9). The metal content of **1/SiRAlOx** determined by ICP-MS was 2.0 wt% Fe and 5.6 wt% Ni. The catalytic activity of **1/SiRAlOx** was evaluated

for magnetically-induced CO_2 hydrogenation in an up-flow set-up (see Experimental section for details). Catalytic tests were performed in a glass flow reactor using a H_2/CO_2 molar ratio of 4/1 and 400 mg of catalyst under atmospheric pressure and with a total flow rate of 25 $mL \cdot min^{-1}$ (49 $L \cdot h^{-1} \cdot g_{(Fe+Ni)}^{-1}$), varying the magnetic field amplitude between 19 and 65 mT (see Fig 2). At 19 mT, the global reactor temperature was ca. 410 °C and a CO_2 conversion of 38 % was obtained, with a 65% CH_4 selectivity. The large presence of CO confirms that CO_2 methanation follows a two-step mechanism where, CO_2 is first hydrogenated into CO and H_2O, through the so-called reverse water gas-shift reaction (RWGS), followed then by the exothermic CO methanation. At 25 mT, the reaction temperature increased to ca. 520°C leading to a 71% CO_2 conversion. However, the CH_4 selectivity considerably dropped from 65% down to 50%. Regarding the mechanism proposed, high temperatures promote the RWGS explaining the increase of CO_2 conversion, but at the same time they shift the equilibrium of exothermic CO methanation toward the CO production, thus decreasing the selectivity.[38] Further increase of the magnetic field amplitude up to 65 mT led to similar temperatures and hence conversion rates.

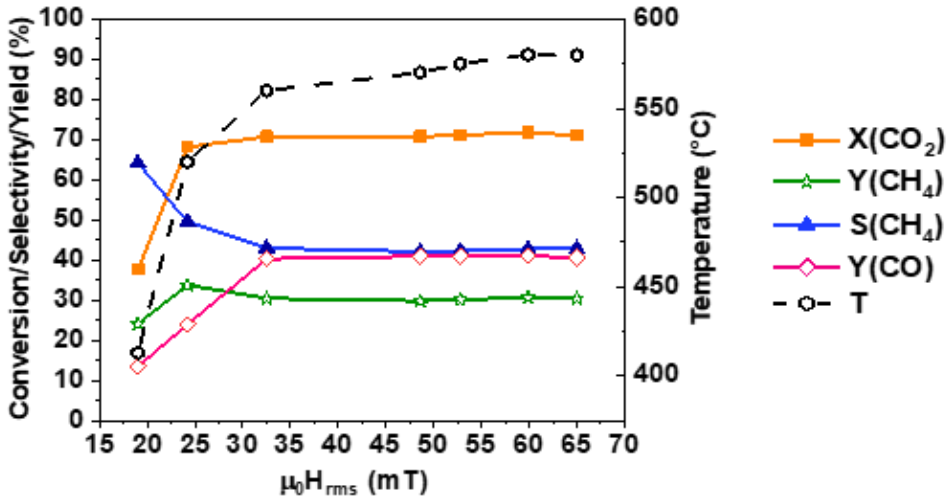

Figure 2. Magnetically induced CO_2 hydrogenation in an up-flow reactor using 400 mg of **1/SiRAlOx** as catalyst (ratio H_2/CO_2=4/1, 25 $mL \cdot min^{-1}$, 49 $L \cdot h^{-1} g_{(Fe+Ni)}^{-1}$).

We attribute the reduced CH_4 selectivity of **1/SiRAlOx** to the presence of the Fe-rich shell, previously evidenced by advanced spectroscopies. Therefore, we chemically modified the NP surface by decomposing 0.4 eq. Ni[^{i}PrNC(CH$_3$)N^{i}Pr]$_2$ per total metal under H_2 in the presence of NPs **1** (see Scheme 2), to yield $Fe_{30}Ni_{70}$@Ni NPs (**2**). TEM micrographs showed that the mean sizes of the NPs slightly increased from 17.3 ± 2.2 to 18.6 ± 2.4 nm (Figure 3a). HR-TEM analyses revealed that NPs **2** are polycrystalline and exhibit the *fcc* structure (Figure 3b). STEM-EDX analyses suggest that the NP surface was enriched in Ni, but discarding the formation of a complete Ni shell (Fig 3c-d).

When comparing structural characterization of **1** and **2** (see Fig 1a-b), no significant differences were observed neither in the XRD patterns nor in the static magnetic properties measured by VSM at 300 K (see also Fig S10 for VSM at 5 K). However, the SAR of the NPs **2** dropped from 600 to 350 W.g^{-1} after Ni enrichment (see Fig 1c), as expected after the addition of a *softer* material such as Ni.[39]

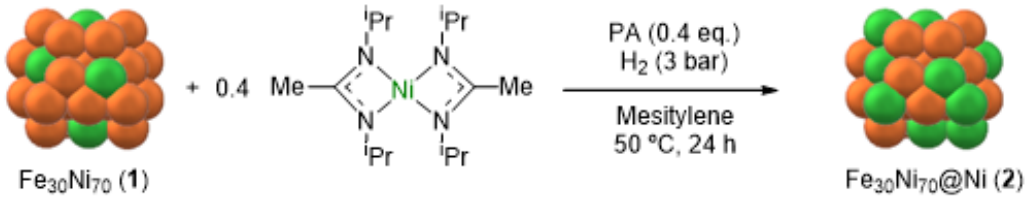

Scheme 2. Synthesis of $Fe_{30}Ni_{70}$ NPs **2** by decomposition of Ni[^{i}PrNC(CH$_3$)N^{i}Pr]$_2$ under a H_2 atmosphere in the presence of **1**

NPs **2** were supported on SiRAlOx (see Fig S11) and evaluated for CO_2 hydrogenation. As expected, **2/SiRAlOx** displayed a slightly higher amount of Ni by ICP-MS than NPs **1/SiRAlOx** (6.1 wt% vs. 5.6 wt% respectively), but a comparable Fe content (2.0 wt% vs. 1.8 wt%). Interestingly, despite **2** displayed lower values of SAR, the reaction temperatures as a function of the magnetic field amplitude were comparable to those measured for **1/SiRAlOx**

under similar reaction conditions (400 mg of catalyst, 25 $mL \cdot min^{-1}$ of a 4:1 H_2:CO_2 molar mixture, 47 $L \cdot h^{-1} \cdot g_{(Fe+Ni)}^{-1}$, see Fig S12). However, the catalytic performances increased considerably, which is a clear proof of the surface enrichment with Ni. For instance, at 24 mT, a 72 % of CO_2 conversion was obtained with a 92% selectivity to CH_4. The CO_2 conversion reached 82% at an applied field of 44 mT. CH_4 yields were found between 65 and 75% in all the cases.

The catalytic performances were notably improved by increasing the residence time of the gas flow, performing the reaction with 800 mg of **2/SiRAlOx** (24 $L \cdot h^{-1} \cdot g_{(Fe+Ni)}^{-1}$, see Figure S13). At 13 mT, 75 % of CO_2 is selectively converted into CH_4. When the magnetic field amplitude was set to 19 mT, we could remarkably achieve the complete conversion of CO_2 into CH_4.

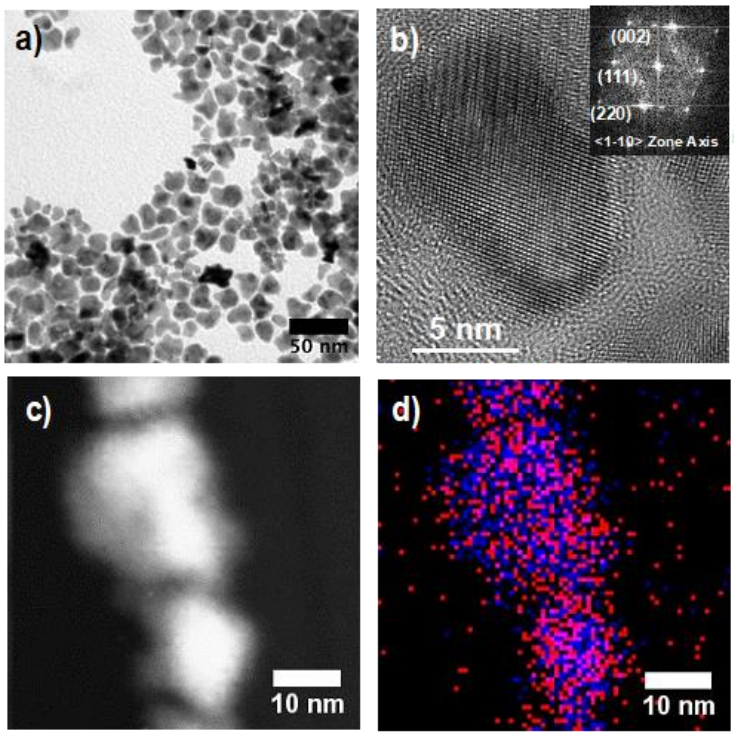

Figure 3. a) Conventional TEM and b) HR-TEM images of NPs **2**. c-d) STEM-EDX elemental mapping of NPs **2** (Fe atoms in red and Ni atoms in blue).

Nevertheless, the up-flow reactor led to an accumulation of water in the water trap (see Fig S14), which can reflux to the catalyst, and hence reduce the catalytic performance of the powder on a long-term basis. We therefore optimized the experimental set-up to a down-flow reactor, and to ensure an optimal fluidization of the gas-flow, 400 mg of SiC were added to the 800 mg of **2/SiRAlOx** keeping the other parameters constant (24 $L \cdot h^{-1} \cdot g_{(Fe+Ni)}^{-1}$). A reaction profile is shown in Fig 4. In this case, the reaction temperatures were considerably lower due to the dilution with SiC (375°C vs 470°C). Therefore slightly higher magnetic field amplitudes were required to activate the reaction. At 18 mT, CO_2 conversion increased to 85% with a 100% selectivity to CH_4 and at 22 mT or higher, full CO_2 conversion was observed. The TOF was estimated to ca. 620 h^{-1} taking into account NPs size and the proportion of surface atoms. The system was highly stable in time and the reaction profile was not affected by stopping the coil and starting again. In addition, we can propose that the reaction is in the kinetic regime, as conversions and yields are almost independent on the reactor geometry at low flow rate when maintaining constant mean temperatures of 410 ºC, (Fig S15).

Thus, the improvement of the reaction profile in the down-flow set-up relies on the efficient water removal from the medium. NPs **2/SiRAlOx** were characterized by STEM-EDX at the end of the reaction (Figure S16). Most of the NPs were sintered as observed with the catalytic system composed by $Fe_{2.2}C$ NPs supported on Ni/SiRAlOx previously reported in our group,[5] but interestingly, their optimized catalytic performances are preserved. Finally, stability of NPs **2/SiRAlOx** was evaluated. After 8 hours on stream at 22 mT, CO_2 conversion values were of 97% with a 99% selectivity to CH4, showing the robustness of the system (energy efficiency of $2.86 \cdot 10^{-6}$ mol $CO_2 \cdot kJ^{-1}$).

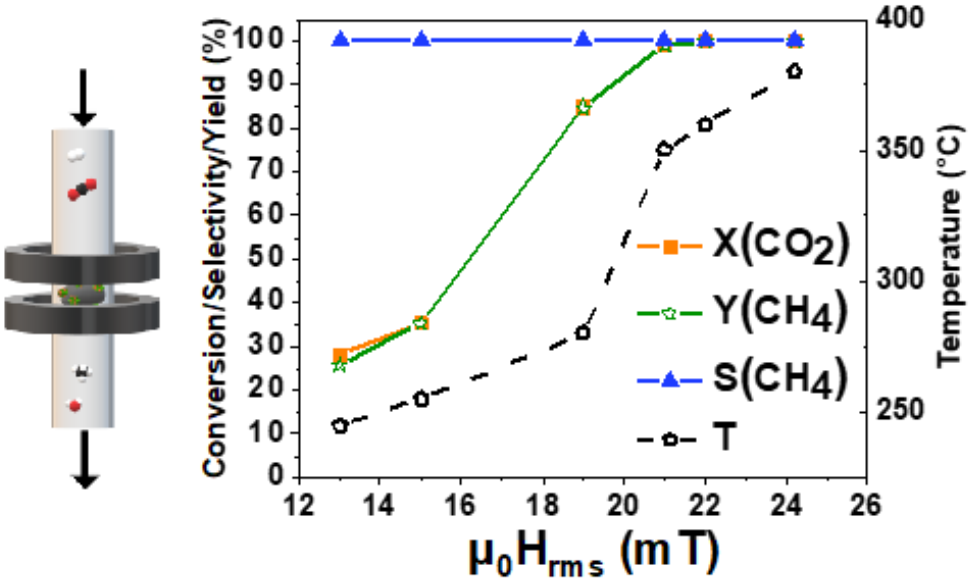

Figure 4. Magnetically induced CO_2 methanation in a down-flow reactor using **2/SiRAlOx** catalyst (ratio H_2/CO_2=4/1, 25 mL·min^{-1}, 24 L·h^{-1}·g$_{(Fe+Ni)}^{-1}$).

Overall, we report here the synthesis of FeNi NPs of controllable composition. The optimum Fe30Ni70 NPs display good heating properties at low magnetic field, thanks to their reduced magnetocrystalline anisotropy[36] but lead to moderate conversions for magnetically-induced CO2 methanation due to their Fe-rich surface. Upon further deposition of Ni onto the NPs surface, we were able to obtain the full CO_2 conversion into CH_4. Thus, engineering the surface of FeNi NPs permits to combine in a single nano-object high heating powers and excellent catalytic activity. It should be mentioned that even though the SAR of the catalytic systems based on $Fe_{30}Ni_{70}$@Ni were below those previously reported for $Fe_{2.2}C$@Ni NPs (SAR of ca. 350 W·g-1 vs. 1000 W·g^{-1} measured at 47 mT and 93 kHz),[23, 40] $Fe_{30}Ni_{70}$@Ni display much higher catalytic activity under comparable reaction conditions. The use of lower magnetic field amplitudes is a strong improvement of the energy efficiency of the system. $Fe_{30}Ni_{70}$@Ni NPs are therefore catalysts of choice for magnetic methanation working at low field amplitude and accessible through an easy and scalable synthesis. The full conversion, above the thermodynamic equilibrium, presumably originates from the out-of-equilibrium nature of

magnetically induced catalysis resulting from high temperature gradients within the reactor that permit efficient water removal and thus shift the reaction equilibrium.

CONCFLICTS OF INTEREST

The authors declare no conflict of interest

AKNOWLEDGMENTS

The authors thank ERC Advanced Grant (MONACAT 2015-694159) for financial support.

REFERENCES

[1] S. Chatterjee, V. Degirmenci, E. V. Rebrov, *Chem. Eng. J.* **2015**, *281*, 884–891.

[2] A. Meffre, B. Mehdaoui, V. Connord, J. Carrey, P. F. Fazzini, S. Lachaize, M. Respaud, B. Chaudret, *Nano Lett.* **2015**, *15*, 3241–3248.

[3] A. Bordet, L. M. Lacroix, K. Soulantica, B. Chaudret, *ChemCatChem* **2016**, *8*, 1727–1731.

[4] A. Bordet, L. M. Lacroix, P. F. Fazzini, J. Carrey, K. Soulantica, B. Chaudret, *Angew. Chemie - Int. Ed.* **2016**, *55*, 15894–15898; *Angew.Chemie.* **2016**, *128,* 16126-16130.

[5] S. S. Kale, J. M. Asensio, M. Estrader, M. Werner, A. Bordet, P. Fazzini, D. Yi, J. Marbaix, K. Soulantica, B. Chaudret, *Catal. Sci. Technol.* **2019**, *9*, 2601–2607.

[6] A. Bordet, J. M. Asensio, K. Soulantica, B. Chaudret, *ChemCatChem* **2018**, *10*, 4047–4051.

[7] L. Huang, A. Shan, Z. Li, C. Chen, R. Wang, *CrystEngComm* **2013**, *15*, 2527–2531.

[8] W. Wang, C. Duong-Viet, Z. Xu, H. Ba, G. Tuci, G. Giambastiani, Y. Liu, T. Truong-Huu, J. M. Nhut, C. Pham-Huu, *Catal. Today* **2019**, 1–7.

[9] W. Wang, G. Tuci, C. Duong-Viet, Y. Liu, A. Rossin, L. Luconi, J.-M. Nhut, L. Nguyen-Dinh, C. Pham-Huu, G. Giambastiani, *ACS Catal.* **2019**, *9*, 7921–7935.

[10] A. Ovenston, J. R. Walls, *J. Chem. Soc. Faraday Trans. 1 Phys. Chem. Condens. Phases* **1983**, *79*, 1073–1084.

[11] T. Koch, K. Krause, M. Mehdizadeh, K. Sengupta, B. Blackwell, *Induction Heated Reactor Apparatus*, **1997**.

[12] J. Leclercq, F. Giraud, D. Bianchi, K. Fiaty, F. Gaillard, *Appl. Catal. B Environ.* **2014**, *146*, 131–137.

[13] Y. Liu, N. Cherkasov, P. Gao, J. Fernández, M. R. Lees, E. V Rebrov, *J. Catal.* **2017**, *355*, 120–130.

[14] Y. Liu, P. Gao, N. Cherkasov, E. V Rebrov, *RSC Adv.* **2016**, *6*, 100997– 101007.

[15] M. G. Vinum, M. R. Almind, J. S. Engbæk, S. B. Vendelbo, M. F. Hansen, C. Frandsen, J. Bendix, P. M. Mortensen, *Angew. Chemie - Int. Ed.* **2018**, *57*, 10569–10573; *Angew. Chemie.* **2018**, *130,* 10729-110733.

[16] P. M. Mortensen, J. S. Engbæk, S. B. Vendelbo, M. F. Hansen, M. Østberg, *Ind. Eng. Chem. Res.* **2017**, *56*, 14006–14013.

[17] F. Varsano, M. Bellusci, A. La Barbera, M. Petrecca, M. Albino, C. Sangregorio, *Int. J. Hydrogen Energy* **2019**, *44*, 21037–21044.

[18] S. Ceylan, L. Coutable, J. Wegner, A. Kirschning, *Chem. Eur. J.* **2011**, *17*, 1884–1893.

[19] J. Hartwig, S. Ceylan, L. Kupracz, L. Coutable, A. Kirschning, *Angew. Chemie - Int. Ed.* **2013**, *52*, 9813–9817; *Angew. Chemie.* **2013**, *125,* 9995-9999.

[20] A. Kirschning, L. Kupracz, J. Hartwig, *Chem. Lett.* **2012**, *41*, 562–570.

[21] S. Ceylan, C. Friese, C. Lammel, K. Mazac, A. Kirschning, *Angew. Chemie - Int. Ed.* **2008**, *47*, 8950–8953; *Angew. Chemie.* **2008**, *120,* 9083-9086.

[22] J. M. Asensio, A. B. Miguel, P.-F. Fazzini, P. W. N. M. van Leeuwen, B. Chaudret, *Angew. Chemie - Int. Ed.* **2019**, *131*, 11428–11432; *Angew. Chemie.* **2019**, *131,* 11428–11432.

[23] J. Gao, Q. Liu, F. Gu, B. Liu, Z. Zhong, F. Su, *RSC Adv.* **2015**, *5*, 22759– 22776.

[24] P. Frontera, A. Macario, M. Ferraro, P. Antonucci, *Catalysts* **2017**, *7*, 59.

[25] M. Götz, J. Lefebvre, F. Mörs, A. McDaniel Koch, F. Graf, S. Bajohr, R. Reimert, T. Kolb, *Renew. Energy* **2016**, *85*, 1371–1390.

[26] T. Bligaard, J. K. Nørskov, S. Dahl, J. Matthiesen, C. H. Christensen, J. Sehested, *J. Catal.* **2004**, *224*, 206–217.

[27] M. P. Andersson, T. Bligaard, A. Kustov, K. E. Larsen, J. Greeley, T. Johannessen, C. H. Christensen, J. K. Nørskov, *J. Catal.* **2006**, *239*, 501–506.

[28] A. L. Kustov, A. M. Frey, K. E. Larsen, T. Johannessen, J. K. Nørskov, C. H. Christensen, *Appl. Catal. A Gen.* **2007**, *320*, 98–104.

[29] D. Tian, Z. Liu, D. Li, H. Shi, W. Pan, Y. Cheng, *Fuel* **2013**, *104*, 224– 229.

[30] Q. Liao, R. Tannenbaum, Z. L. Wang, *J. Phys. Chem. B* **2006**, *110*, 14262–14265.

[31] Y. Liu, Y. Chi, S. Shan, J. Yin, J. Luo, C. J. Zhong, *J. Alloys Compd.* **2014**, *587*, 260–266.

[32] O. Margeat, D. Ciuculescu, P. Lecante, M. Respaud, C. Amiens, B. Chaudret, *Small* **2007**, *3*, 451–458.

[33] C. Garnero, M. Lepesant, C. Garcia-Marcelot, Y. Shin, C. Meny, P. Farger, B. Warot-Fonrose, R. Arenal, G. Viau, K. Soulantica, et al., *Nano Lett.* **2019**, *19*, 1379–1386.

[34] B. Mehdaoui, A. Meffre, J. Carrey, S. Lachaize, L.-M. Lacroix, M. Gougeon, B. Chaudret, M. Respaud, *Adv. Funct. Mater.* **2011**, *21*, 4573– 4581.

[35] E. Lima, V. Drago, J. C. De Lima, P. F. P. Fichtner, *J. Alloys Compd.* **2005**, *396*, 10–17.

[36] B. D. Cullity ; C. D. Graham, *Introduction to Magnetic Materials*, **2009**.

[37] J. Nogués, I. K. Schuller, *J. Magn. Magn. Mater.* **1999**, *192*, 203–232.

[38] I. Champon, A. Bengaouer, A. Chaise, S. Thomas, A. C. Roger, *J. CO2 Util.* **2019**, *34*, 256–265.

[39] J. M. Asensio, J. Marbaix, N. Mille, L. Lacroix, K. Soulantica, P. Fazzini, J. Carrey, B. Chaudret, *Nanoscale* **2019**, *11*, 5402–5411.